Applied Catalysis B: Environmental 150–151 (2014) 298–304

Contents lists available at ScienceDirect

Applied Catalysis B: Environmental

journal homepage: www.elsevier.com/locate/apcatb

Ni/reduced graphene oxide nanocomposite as a magnetically recoverable catalyst with near infrared photothermally enhanced activity

Chun-Chieh Yeh, Dong-Hwang Chen*

Department of Chemical Engineering, National Cheng Kung University, Tainan 701, Taiwan

ARTICLE INFO

Article history:
Received 30 September 2013
Received in revised form 3 December 2013
Accepted 20 December 2013
Available online 28 December 2013

Keywords:
Ni nanoparticles
Reduced graphene oxide
Magnetically recoverable catalyst
Near infrared photothermally enhancement
4-Nitrophenol

ABSTRACT

A nanocomposite of nickel nanoparticles/reduced graphene oxide (Ni/rGO) has been developed as a magnetic recoverable catalyst with near-infrared (NIR) photothermally enhanced activity owing to the magnetic and catalytic properties of Ni nanoparticles as well as the large specific surface area and excellent NIR photothermal conversion property of rGO. By the hydrazine reduction in ethylene glycol, Ni ions, and graphene oxide were reduced simultaneously to form the Ni/rGO nanocomposite. The resulting Ni/rGO nanocomposite with about 62 wt.% of Ni nanoparticles was nearly superparamagnetic and possessed good catalytic activity toward the reduction of 4-nitrophenol (4-NP) to 4-aminophenol (4-AP) with sodium borohydride. The corresponding pseudo-first-order rate constants increased with increasing the temperature and 4-NP concentration, revealing activation energy of 43.7 kJ/mol and the synergistic effect of rGO. Furthermore, under NIR irradiation, it was demonstrated that the Ni/rGO could efficiently enhance the reduction rate via the photothermal conversion which might induce the heating of local environment around the Ni nanoparticles and reaction medium. Such a nanocomposite was expected to be helpful in the development of NIR or solar photothermally enhanced catalytic systems.

1. Introduction

4-Nitrophenols (4-NP) is a common organic pollutant in wastewater. A lot of processes have been developed for its removal, such as adsorption, microbial degradation, photocatalytic degradation, electro–Fenton method, electrocoagulation, electrochemical treatment, and so on [1]. Moreover, 4-NP is also a common precursor of 4-aminophenol (4-AP) which is renowned as a kind of useful material in many applications that involve corrosion inhibitor, analgesic/antipyretic drugs, photographic developer, anticorrosion lubricant, hair-dyeing agent [2–4]. So, considerable efforts have been made on the reduction of 4-NP to 4-AP. In the past two decades, the borohydride reduction of 4-NP to 4-AP by metal nanoparticles such as Au, Ag, Pt, Pd, Pt–Ni, and Ni has received increasing attention because this reaction can be performed in aqueous solution under mild condition [5–11].

On the other hand, graphene which is a single or few layer of 2-dimensional graphite carbon sheets has attracted great interest recently in various fields of science and engineering owing to its high surface area, unique optical property, and good electrical, thermal and mechanical properties [12–16]. Although a lot of methods have been developed for the preparation of graphene sheets, the most suitable and efficient approach was the solution-based chemical reduction of exfoliated graphite oxide to reduced graphene oxide (rGO) because of its low-cost and facile synthetic nature in a controlled, scalable, and reproducible manners [17,18]. Graphite oxide can be readily dispersed in water to yield the stable dispersions of graphene oxide (GO) by simple sonication owing to the presence of oxygen-containing functional groups such as hydroxyl, epoxide, and carboxyl moieties [19]. Furthermore, these oxygen functional groups can act as nucleation centers or anchoring sites for the attachment of nanoparticles [20], which limited the growth of nanoparticles and improved the stability and dispersion of nanoparticles on GO or rGO. These nanoparticles can also help to enlarge the interplanar spacing of the GO or rGO in solid state, maintain the excellent properties of individual GO or rGO sheets, and avoid the aggregation of GO or rGO sheets into graphitic structure [11,21]. On the basis of the above advantages, GO and rGO have been widely used as the supports for the attachment of nanoparticles to yield the nanocomposites for various applications, particularly in the catalysis [22–24].

It was mentionable, recently we demonstrated that LaB_6 nanoparticles possessed excellent near infrared (NIR) photothermal conversion property and could be used in the NIR photothermal

* Corresponding author at: National Cheng Kung University, Department of Chemical Engineering, No 1, Ta-Hsueh Rd, Tainan 701, Taiwan.
Tel.: +886 6 2757575x 6268; fax: +886 6 2344496.
E-mail address: chendh@mail.ncku.edu.tw (D.-H. Chen).

0926-3373/$ – see front matter © 2013 Elsevier B.V. All rights reserved.
http://dx.doi.org/10.1016/j.apcatb.2013.12.040

therapy of cancer therapy and the photothermal ablation of bacteria [25–27]. Also, after silica coating and Au nanoparticles deposition, the resulting LaB_6@SiO_2/Au composite nanoparticles were efficient for the catalytic reduction of 4-NP with $NaBH_4$ and the reduction rate of 4-NP could be enhanced by NIR irradiation because they not only induced the heating of reaction medium but also provided hot spots on the catalyst surface via the photothermal conversion [28]. Graphene and rGO also possess the excellent NIR photothermal conversion property and have been used in NIR photothermal therapy [29–31]. Although graphene-based sheets have been widely used as the catalyst supports, their application in the photothermally enhancement of catalytic reaction rate by NIR irradiation has not been reported.

According to the above, the nanocomposite of Ni nanoparticles and rGO (Ni/rGO) was fabricated for the catalytic reduction of 4-NP to 4-AP in this work. Ni nanoparticles were chosen because they were cheaper as compared to other noble metal catalysts Au, Ag, Pt, and Pd. Also, the magnetic property of Ni nanoparticles could make the nanocomposite magnetically recoverable. The rGO was used as the support because of its large surface area, suitability for the deposition of nanoparticles, and excellent NIR photothermal conversion property. Such a catalyst with NIR photothermally enhanced activity might be helpful for the development of more efficient catalytic systems with less electrical thermal input. Moreover, although the synthesis of Ni/rGO nanocomposite has been reported, longer reaction time, higher reaction or heat treatment temperature, and/or inert atmosphere were usually required [11,32–36]. Also, only quite few effort has been made on its use in the catalytic reduction of 4-NP [11]. In this work, by the hydrazine reduction in ethylene glycol at a relatively low temperature (i.e., 70 °C), Ni ions and graphene oxide were reduced simultaneously to form the Ni/rGO nanocomposite within 30 min without the input of an extra inert gas. It was demonstrated that the Ni/rGO nanocomposite was magnetically recoverable and efficient for the catalytic reduction of 4-NP to 4-AP with $NaBH_4$. Also, the rGO not only enhanced the catalytic activity via a synergistic effect but also could enhance the reduction rate by NIR irradiation.

2. Materials and methods

2.1. Materials

Graphite powder (99.9%) was a product of Bay Carbon. Nickel chloride was obtained from Riedal-de Haën. Ethylene glycol and sodium hydroxide were supplied by J. T. Baker. Hydrazine hydrate solution (80%) was purchased from Sigma–Aldrich. 4-Nitrophenol and sodium borohydride were obtained from Alfa Aesar and Aldrich, respectively. The above and other chemicals were all of guaranteed or analytical grade reagents commercially available and used without further purification. The water used throughout this work was reagent grade, produced by a Milli-Q SP Ultra-Pure-Water Purification System of Nihon Millipore Ltd., Tokyo.

2.2. Preparation of GO

GO was prepared from purified natural graphite by a modified Hummers' method [11,37]. The graphite powder (1.5 g) and $NaNO_3$ (0.75 g) were added to the concentrated H_2SO_4 (18 M, 37 mL) in an ice-bath. $KMnO_4$ (4.5 g) was added gradually under stirring. The mixture was then stirred at 35 °C for 24 h. Then the deionized water (70 mL) was slowly added to the mixture, followed by stirring the mixture at 98 °C for 15 min. The suspension was further diluted to 110 mL and stirred for another 30 min. The reaction was terminated by adding H_2O_2 (3.7 mL, 35 wt.%) under stirring at room temperature, followed by washing with the deionized water several times.

2.3. Preparation of Ni/rGO nanocomposite

Ni/rGO nanocomposite was synthesized according to our previous work on the synthesis of Ni nanoparticles [38]. Typically, firstly, GO (5 mg) was dispersed in ethylene glycol (7.5 mL) with ultrasonication for 30 min and then mixed with the ethylene glycol of $NiCl_2$ (100 mM, 7.5 mL) to yield a homogeneous brown solution. Secondly, an appropriate amount of NaOH (1.0 M) was added to adjust the pH to about 10.5 and then hydrazine solution (80%, 0.7 mL) was added under continuous stirring. Finally, the reaction was conducted at 70 °C for 30 min to yield a homogeneous black solution. The product was recovered magnetically by a magnet, washed with ethanol for three times, and then dried in an oven at 40 °C. For comparison, Ni nanoparticles and rGO were prepared according to the above procedures in the absence of GO or $NiCl_2$, respectively.

2.4. Characterization

The particle size and composition were determined by transmission electron microscopy (TEM) and energy dispersive X-ray (EDX) spectroscopy on a high-resolution field emission transmission electron microscopy (HRTEM, JEOL Model JEM-2100F). The high-resolution TEM (HRTEM) image and selected area electron diffraction (SAED) pattern were obtained by a JEOL Model JEM-2100F electron microscope at 200 kV. The crystalline structures were characterized by X-ray diffraction (XRD) analysis on a Shimadzu model RX-III X-ray diffractometer at 40 kV and 30 mA with Cu Kα radiation (λ = 0.1542 nm). Raman scattering was performed on a Thermo Fisher Scientific DXR Raman Microscopy using a 532 nm laser source. The XPS measurements were performed on a KRATOS AXIS Ultra DLD photoelectron spectrophotometer with an achromatic Mg/Al X-ray source at 450 W. Magnetic measurement was performed on a superconducting quantum interference device (SQUID) magnetometer (MPMS7, Quantum Design). The absorption spectra were analyzed using a JASCO V-570 UV–vis spectrophotometer.

2.5. Catalytic reduction of 4-nitrophenol

For the catalytic reduction of 4-NP, typically, an appropriate amount of Ni/rGO nanocomposite was added to the aqueous solution containing 4-NP and $NaBH_4$ at the desired temperature to start the reaction. The bright yellow color of solution gradually vanished, indicating the reduction of 4-NP. The variation of 4-NP concentration with time was monitored spectrophotometrically at a wavelength of 400 nm. Unless specified otherwise, the initial concentration of 4-NP was 0.05 mM and the reaction temperature was 25 °C. The initial concentration ratio of $NaBH_4$ to 4-NP was fixed at 100 so that the concentration of $NaBH_4$ could be considered as a constant during the reaction. The concentration of Ni/rGO nanocomposite in the reaction solution was 0.01 mg/mL and the solution volume was 3.0 mL throughout this work. For comparison, the catalytic reduction of 4-NP with $NaBH_4$ by rGO or Ni nanoparticles was also examined. For the NIR photothermally enhanced catalytic reduction of 4-NP, the reaction was performed under NIR irradiation by a CW 808 nm diode laser at a power density 5.42 W/cm^2. During the reaction, the temperature was also detected with a thermal couple to examine the temperature variation. To demonstrate the adsorption of 4-NP on rGO, an adsorption experiment was conducted in the solution (3 mL) containing 4-NP (0.05 mM) and rGO (0.01 mg/mL) in the absence of $NaBH_4$ at 25 °C. After about 25 min, the 4-NP concentration in the solution was determined spectrophotometrically at a wavelength of 317 nm.

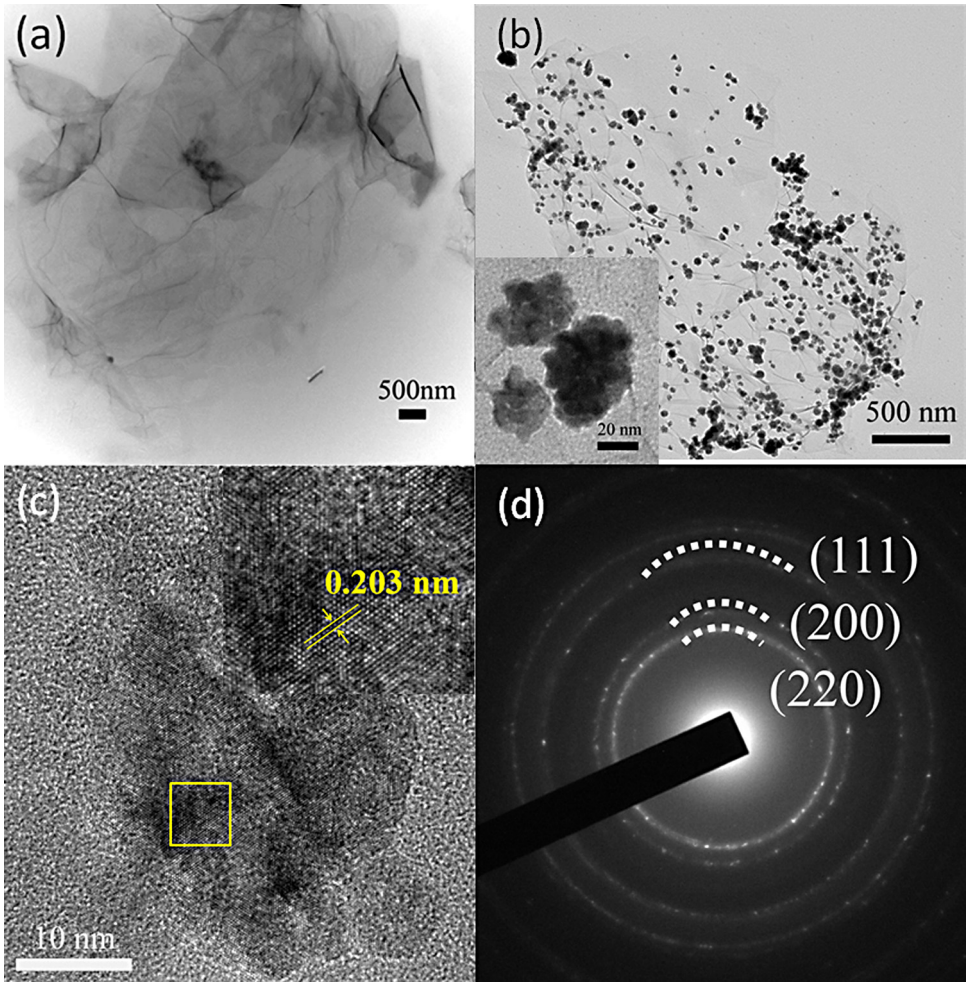

Fig. 1. (a) TEM image of rGO, (b) TEM image, (c) HRTEM image, and (d) SAED pattern of Ni/rGO nanocomposites. The inset in (b) is the magnified image of Ni/rGO nanocomposite. The inset in (c) is the magnified image for the marked square area.

For the reusability study, Ni/rGO nanocomposite was recovered magnetically, washed with deionized water, and then reused. The 4-NP concentration was 0.05 mM and the initial concentration ratio of $NaBH_4$ to 4-NP was also fixed at 100. However, the concentration of Ni/rGO nanocomposite was raised to 0.1 mg/mL to diminish the effect of mass loss during the recovery/washing process.

3. Results and discussion

3.1. Basic properties of Ni/rGO nanocomposite

Fig. 1a and b shows the typical TEM images of rGO and Ni/rGO nanocomposite. It was obvious that the Ni nanoparticles of about 30 nm were formed on rGO. From the inset of Fig. 1b, it could be further observed that these Ni nanoparticles were the agglomerates of smaller Ni nanoparticles. The corresponding HRTEM image was shown in Fig. 1c. An interlayer spacing of 0.203 nm which related to the (1 1 1) plane of face-centered cubic (fcc) nickel could be observed. Furthermore, the SAED pattern as indicated in Fig. 1d showed the characteristic rings for the (1 1 1), (2 0 0), and (2 2 0) planes of fcc nickel. Both the results revealed the Ni nanoparticles decorated on rGO had the fcc structure. By EDX analysis as indicated in Fig. 2, the presence of Ni element confirmed the deposition of Ni nanoparticles. Also, the weight percentage of Ni in the product was determined to be 62%.

Fig. 3 shows the XRD patterns of GO, rGO, Ni, and Ni/rGO nanocomposite. The characteristic peaks of GO and rGO were observed at about $2\theta = 10.5$ and 23.0°, respectively, confirming GO has been reduced to rGO successfully by hydrazine. For Ni nanoparticles, three main characteristic peaks at $2\theta = 44.6$, 52.1, and 76.6° corresponding to the (1 1 1), (2 0 0), and (2 2 2) planes of fcc nickel were observed. For Ni/rGO, three characteristic peaks of Ni and a broad characteristic peak of rGO around 23° was observed, confirming the simultaneous reduction of Ni^{2+} ions and GO. In addition, by using Scherrer equation [39], the grain sizes of Ni nanoparticles on rGO could be estimated to be 3.3 nm. This was consistent with the

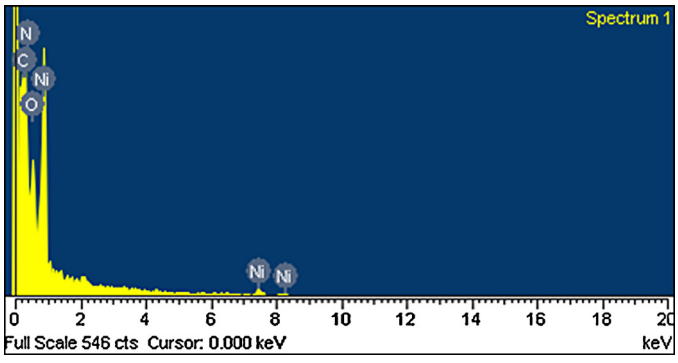

Fig. 2. EDX spectrum of Ni/rGO nanocomposite.

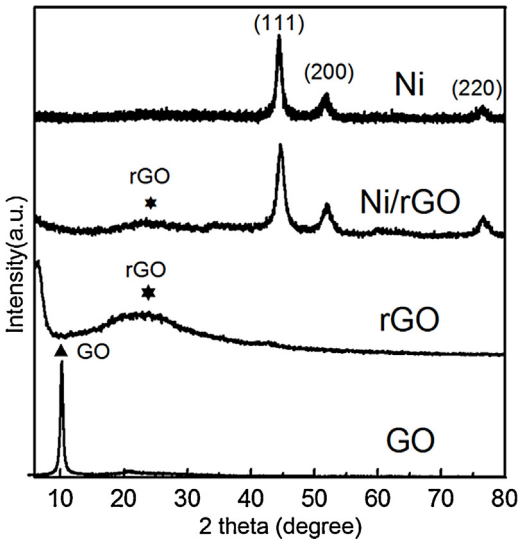

Fig. 3. XRD patterns of GO, rGO, Ni, and Ni/rGO nanocomposite.

above TEM observation and revealed that the smaller Ni nanoparticles of about 3.3 nm were agglomerated to the larger agglomerates of about 30 nm on the surface of rGO.

The Raman spectra of GO, rGO, and Ni/rGO nanocomposite were shown in Fig. 4. Two prominent peaks corresponding to the G and D bands were observed clearly. The G band is usually assigned to the E_{2g} phonon of C sp^2 atoms, while the D band originates from breathing κ-point phonon with A_{1g} symmetry and related to local defects and disorders [40–42]. The intensity ratio of D band to G band (I_D/I_G) is correlative with the average size of sp^2 domains [43]. Higher I_D/I_G ratio means the smaller size of sp^2 domains. From Fig. 4, the I_D/I_G ratios for GO, rGO and Ni/rGO were 0.775, 1.749, and 1.186, respectively. It was reasonable that the I_D/I_G ratios of rGO and Ni/rGO nanocomposite were larger than that of GO because the conjugated graphene network (sp^2 carbon) would be re-established after chemical reduction of GO but the size of the re-established graphene network was usually smaller than the original graphite layer, leading to the increase of I_D/I_G ratio [11,32,33,44]. Because the increase of I_D/I_G ratio was usually resulted by the reduction of GO [11,32,33,43,44], it could be further confirmed that nickel ions and GO were reduced simultaneously. In addition, the I_D/I_G ratio of Ni/rGO nanocomposite was lower than that of rGO. This might be

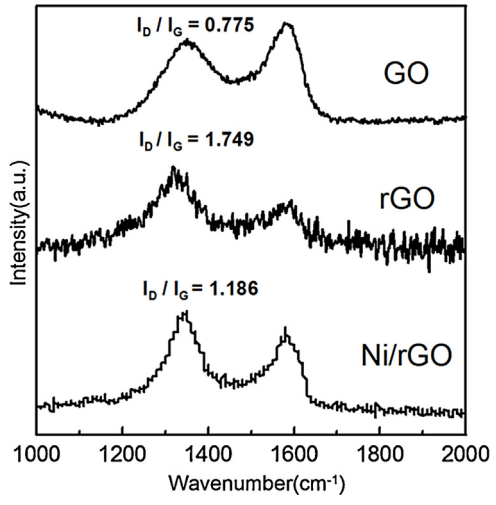

Fig. 4. Raman spectra of GO, rGO, and Ni/rGO nanocomposite.

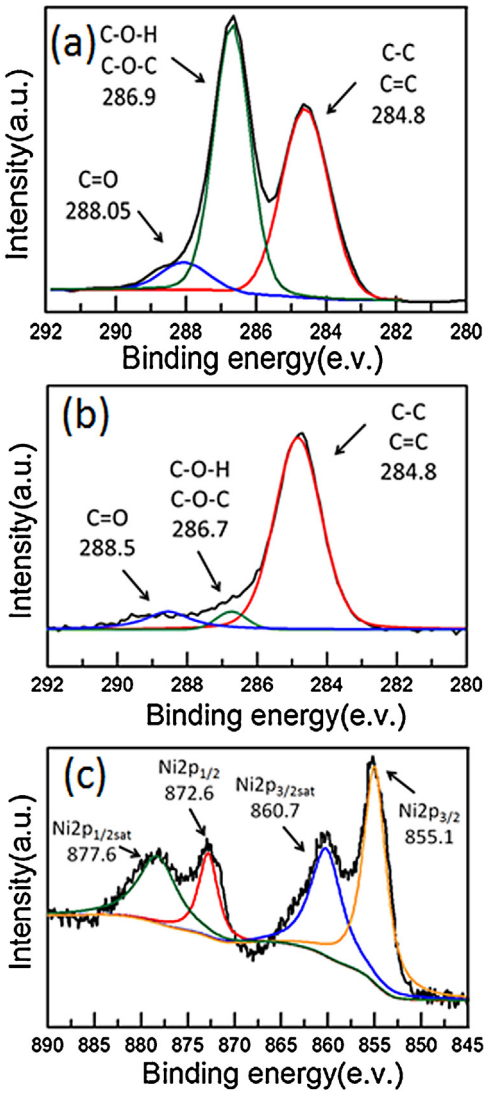

Fig. 5. XPS spectra of (a) C1s of GO and (b) C1s, and (c) Ni2p of Ni/rGO nanocomposite.

due to the local defects and disorders resulted from the decoration of Ni nanoparticles on the surface of rGO.

Fig. 5 shows the XPS spectra of GO and Ni/rGO nanocomposite. In Fig. 5a, the C1s XPS spectrum of GO showed the characteristic peaks of C—C, C=C (at 284.8 eV), C—O—H, C—O—C (at 286.9 eV), and C=O (at 288.05 eV). They could be attributed to the presence of epoxide, hydroxyl, and carboxyl groups [46,47]. In Fig. 6b, the peak intensity of C1s which related to oxygenated functional groups (C—O—H, C—O—C, and C=O) showed a significant decrease, confirming that most of the epoxide, hydroxyl, and carboxyl functional groups were removed and GO has been successfully reduced [46,47]. Fig. 6c shows the XPS signatures of the Ni 2p for the Ni nanoparticles deposited on rGO. The Ni $2p_{1/2sat}$, $2p_{1/2}$, $2p_{3/2sat}$, and $2p_{3/2}$ peaks appeared at 877.6, 872.6, 860.7, and 855.1 eV, respectively. This confirmed the deposition of Ni nanoparticles on the surface of rGO.

The plot of magnetization versus magnetic field (M–H loop) at 25 °C for Ni/rGO nanocomposite was illustrated in Fig. 6. The weak hysteresis revealed that they were nearly superparamagnetic. From the M–H loop and its enlargement near the origin as shown in the lower-right inset of Fig. 6, the saturation magnetization (M_s), remanent magnetization (M_r), coercivity (H_c), and squareness ($S_r = M_r/M_s$) could be determined to be 19.2 emu/g, 5.77 emu/g, 176 Oe, and 0.033, respectively. The upper-left inset

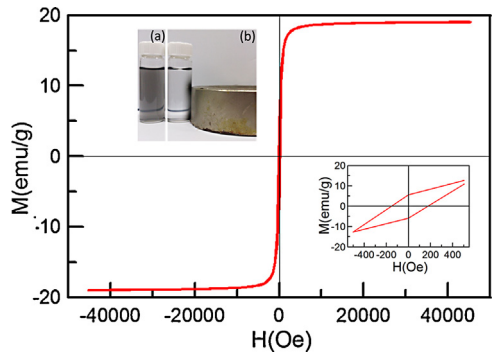

Fig. 6. Magnetization versus magnetic field for Ni/rGO nanocomposite at 25 °C. The lower-right inset is the enlargement near the origin. The upper-left inset is the photographs for the resulting aqueous solution of Ni/rGO nanocomposite (a) without and (b) with a magnet on the outer wall of the vessel.

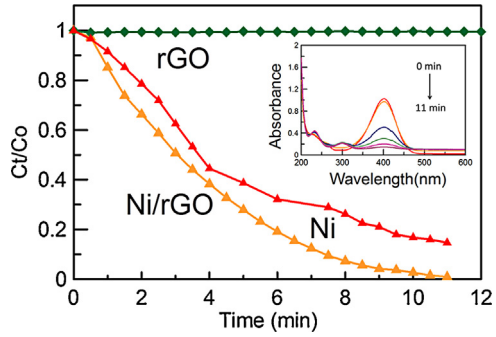

Fig. 7. Plots of C_t/C_0 versus time for the catalytic reduction of 4-NP with $NaBH_4$ by rGO, Ni/rGO nanocomposite, and Ni nanoparticles. The inset indicates the variation of UV–vis absorption spectra with time for the catalytic reduction of 4-NP with $NaBH_4$ by Ni/rGO nanocomposite. (4-NP) = 0.05 mM, ($NaBH_4$)/(4-NP) = 100, 25 °C, catalyst amount: 0.01 mg/mL for rGO and Ni/rGO nanocomposite and 0.0062 mg/mL for Ni nanoparticles.

of Fig. 6 shows the photographs for the resulting aqueous solution of Ni/rGO nanocomposite without and with a magnet on the outer wall of the vessel. It was obvious that the solution was homogeneous and stable, revealing that rGO nanocomposite was well-dispersed in the aqueous solution. Furthermore, by a magnet, rGO nanocomposite could be held on the inner wall completely. This provided a proof that the Ni nanoparticles deposited on the surface of rGO made the nanocomposite magnetically recoverable.

3.2. Catalytic ability of Ni/rGO nanocomposite for 4-NP reduction

To demonstrate the catalytic ability, the reduction of 4-NP (0.05 mM) with $NaBH_4$ at 25 °C in the presence of rGO or Ni/rGO nanocomposite (0.01 mg/mL) was examined. The result was shown in Fig. 7, in which C_0 and C_t denote the concentrations of 4-NP

Table 1
Pseudo-first-order rate constants for the catalytic reduction of 4-NP with $NaBH_4$ by Ni/rGO nanocomposite. Catalyst amount: 0.01 mg/mL, ($NaBH_4$)/(4-NP) = 100.

(4-NP)(mM)	Temperature(°C)	k(min^{-1})	R^2	TOF(mmol/g/s)
0.05	25	0.40	0.9677	0.033
0.05	35	0.63	0.9814	0.053
0.05	45	1.26	0.9931	0.105
0.04	25	0.37	0.9892	0.025
0.06	25	0.51	0.9858	0.051
0.07	25	0.68	0.9638	0.079

when times were 0 and t, respectively. It was obvious that the C_t/C_0 ratio decreased to about zero rapidly within 11 min in the presence of Ni/rGO nanocomposite. The corresponding variation of UV–vis absorption spectra with time was indicated in the inset. However, in the presence of rGO, the C_t/C_0 ratio decreased only quite slightly with time. This revealed that rGO had no significant catalytic ability for the reduction of 4-NP, whereas the Ni/rGO nanocomposite possessed good catalytic ability for the reduction of 4-NP and the catalytic ability was due to the deposited Ni nanoparticles. Furthermore, the catalytic reduction of 4-NP with $NaBH_4$ by Ni nanoparticles has also been studied for comparison. The concentration of Ni nanoparticles used was adjusted to be 0.0062 mg/mL because the Ni content of Ni/rGO nanocomposite was 62 wt.%. As shown in Fig. 7, it was found that the Ni/rGO nanocomposite exhibited a higher catalytic activity than Ni nanoparticles. Because rGO has no significant catalytic activity, this implied that Ni/rGO nanocomposite might have a synergetic effect on the enhancement of catalytic activity as compared to Ni nanoparticles and rGO.

Fig. 8a shows the effect of temperature on the catalytic reduction of 4-NP (0.05 mM) with $NaBH_4$ by Ni/rGO nanocomposite (0.01 mg/mL). It was found that the reaction followed the pseudo-first-order kinetics. The corresponding pseudo-first-order rate constants, R^2, and turnover frequencies (TOF) were listed in Table 1. Obviously, the reduction rate increased with increasing the temperature. By the Arrhenius plot as indicated in Fig. 8b, the activation energy could be calculated to be 43.7 kJ/mol.

Fig. 9 shows the effect of initial 4-NP concentration on the catalytic reduction of 4-NP (0.04–0.1 mM) with $NaBH_4$ by Ni/rGO nanocomposite (0.01 mg/mL) at 25 °C. It was found that the reaction rate increased with increasing the initial 4-NP concentration. The corresponding pseudo-first-order rate constants, R^2, and turnover frequencies were also listed in Table 1. This phenomenon was different from some earlier studies [1] and suggested that the use of rGO as the catalyst support might be helpful for the increase of catalytic activity, showing a synergistic effect [45]. The synergistically enhanced catalytic activity might be explained as follows. Because 4-NP was π-rich in nature, it was expected that 4-NP could be adsorbed onto the surface of rGO via π–π stacking interaction, providing a high 4-NP concentration near the Ni nanoparticles on the surface of rGO and therefore leading to a highly efficient contact between them. The adsorption of 4-NP on rGO nanocomposite

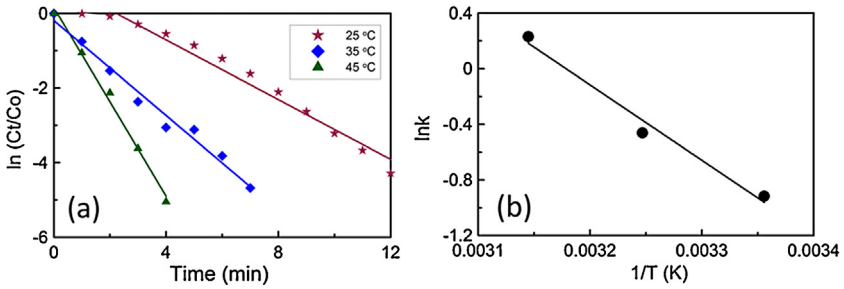

Fig. 8. (a) Plots of ln(C_t/C_0) versus time for the catalytic reduction of 4-NP with $NaBH_4$ by Ni/rGO nanocomposite at different temperatures and (b) the corresponding Arrhenius plot. (4-NP) = 0.05 mM, ($NaBH_4$)/(4-NP) = 100, catalyst amount: 0.01 mg/mL.

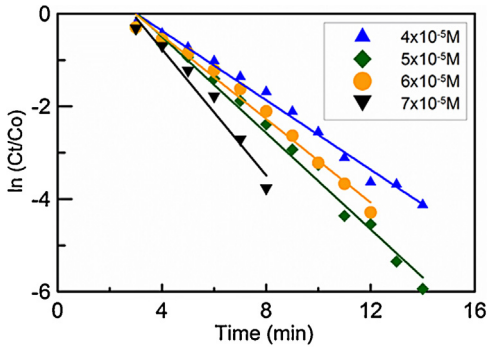

Fig. 9. Plots of $\ln(C_t/C_0)$ versus time for the catalytic reduction of 4-NP with $NaBH_4$ by Ni/rGO nanocomposite at different initial 4-NP concentrations. Catalyst amount: 0.01 mg/mL, 25 °C, $(NaBH_4)/(4\text{-NP}) = 100$.

has been confirmed by the adsorption experiment in the absence of $NaBH_4$. It was found that about 3% of 4-NP could be adsorbed on rGO. For those earlier studies [1,5–10], the catalysts and/or the catalyst supports were usually present in the form of particles. The adsorption of 4-NP on the surface of catalyst support was also not as significant as that on the surface of rGO. So, the reaction occurred mainly via the collision of 4-NP molecules and the catalyst particles, leading to a slower reaction rate [46]. Furthermore, since the work function of graphene (4.48 eV [47,48]) was lower than that of Ni (5.04–5.35 eV [49]), electron transfer from the graphene sheets to Ni nanoparticles might occur [47]. The electron transfer from rGO to Ni nanoparticles also increased the local electron concentration, facilitating the uptake of electrons by 4-NP molecules. Accordingly, for the catalytic reduction of 4-NP to 4-AP with $NaBH_4$ by Ni/rGO nanocomposite, the support rGO could enhance the catalytic activity via a synergistic effect.

Fig. 10 shows the reusability of Ni/rGO nanocomposite (0.1 mg/mL) for the catalytic reduction of 4-NP (0.05 mM) with $NaBH_4$ at 25 °C. It was found that about 80% of the initial catalytic activity was retained after reuse for 7 times, revealing the good stability. This revealed that the Ni/rGO nanocomposite was not deactivated or poisoned significantly.

3.3. Catalytic reduction of 4-NP by Ni/rGO nanocomposite with NIR irradiation

The catalytic reduction of 4-NP with $NaBH_4$ by Ni/rGO nanocomposite under NIR irradiation with and without temperature control at 25 °C was shown in Fig. 11a, in which the reaction at 25 °C without NIR irradiation was also indicated for comparison. It was obvious that the reduction rate of 4-NP with NIR irradiation was faster than that without NIR irradiation. By observing the

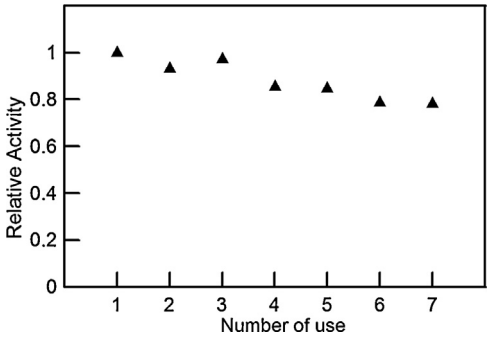

Fig. 10. Reusability of Ni/rGO nanocomposite for the catalytic reduction of 4-NP with $NaBH_4$. $(4\text{-NP}) = 0.05$ mM, $(NaBH_4)/(4\text{-NP}) = 100$, catalyst amount: 0.1 mg/mL, 25 °C.

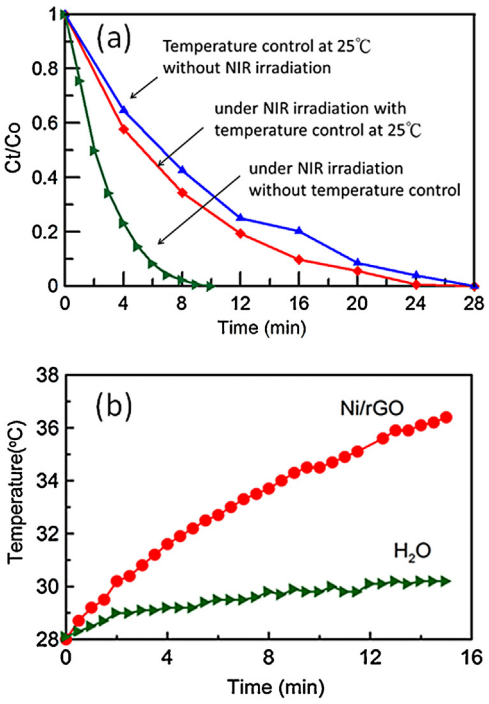

Fig. 11. (a) Plots of C_t/C_0 versus time for the catalytic reduction of 4-NP with $NaBH_4$ by Ni/rGO nanocomposite without NIR irradiation at 25 °C and those under NIR irradiation with and without temperature control at 25 °C. (b) Variations of temperature with time for the reaction solution and water with NIR irradiation. $(4\text{-NP}) = 0.05$ mM, $(NaBH_4)/(4\text{-NP}) = 100$, catalyst amount: 0.01 mg/mL.

temperature variation of reaction medium with time as indicated in Fig. 11b, it was found that the NIR irradiation led to a significant increase of temperature. Under the same NIR irradiation, the temperature increase of water was relatively insignificant. This confirmed the NIR photothermal conversion property of rGO and demonstrated that the catalytic reduction of 4-NP with $NaBH_4$ by Ni/rGO nanocomposite could be enhanced by NIR irradiation. Furthermore, when the reaction was carried out under NIR irradiation with temperature control at 25 °C, the reduction rate was also faster than that without NIR irradiation. This could be attributed to the local temperature effect [28]. Because the heat generated via the NIR photothermal conversion by rGO might transferred to Ni nanoparticles first and then to the surrounding medium, the surface temperature of Ni nanoparticles might be higher than the average temperature of reaction medium. So, NIR irradiation could enhance the reduction rate even the reaction medium was thermostated at 25 °C because the catalytic reaction occurred on the catalyst surface. Thus, the use of rGO as a catalyst support not only provided a large specific surface area and a synergistic effect but also could enhance the catalytic activity via NIR photothermal conversion.

4. Conclusions

Ni/rGO nanocomposite has been fabricated successfully via the hydrazine reduction in ethylene glycol. The Ni nanoparticles of about 3.3 nm were synthesized and agglomerated into larger agglomerates of about 30 nm on the surface of rGO. The deposition of Ni nanoparticles made the nanocomposite magnetically recoverable and efficient for the catalytic reduction of 4-NP to 4-AP with $NaBH_4$. Also, the rGO not only acted as a good support with large specific surface area but also enhanced the catalytic activity of Ni nanoparticles via a synergistic effect. Furthermore, the excellent NIR photothermal conversion property of rGO also made the catalytic reduction of 4-NP by the Ni/rGO nanocomposite could be

enhanced under NIR irradiation. Such a product not only was useful in the waste water treatment and the conversion of 4-NP to 4-AP in aqueous solution under mild condition, but also might be helpful in the development of NIR or solar photothermally enhanced catalytic systems.

Acknowledgement

This work was performed under the auspices of the National Science Council of the Republic of China, under contract number NSC 102-2221-E-006-221-MY3, to which the authors wish to express their thanks.

References

[1] J.R. Chiou, B.H. Lai, K.C. Hsu, D.H. Chen, J. Hazard. Mater. 248 (2013) 394–400.
[2] J.F. Corbett, Dyes Pigm. 41 (1999) 127–136.
[3] C.V. Rode, M.J. Vaidya, R.V. Chaudhari, Org. Process Res. Dev. 3 (1999) 465–470.
[4] Z.Y. Zhang, C.L. Shao, P. Zou, P. Zhang, M.Y. Zhang, J.B. Mu, Z.C. Guo, X.H. Li, C.H. Wang, Y.C. Liu, Chem. Commun. 47 (2011) 3906–3908.
[5] K. Esumi, K. Miyamoto, T. Yoshimura, J. Colloid Interface Sci. 254 (2002) 402–405.
[6] S.K. Ghosh, M. Mandal, S. Kundu, S. Nath, T. Pal, Appl. Catal. A: Gen. 268 (2004) 61–66.
[7] K. Hayakawa, T. Yoshimura, K. Esumi, Langmuir 19 (2003) 5517–5521.
[8] Y. Lu, Y. Mei, M. Schrinner, M. Ballauff, M.W. Moller, J. Phys. Chem. C 111 (2007) 7676–7681.
[9] B. Naik, S. Hazra, V.S. Prasad, N.N. Ghosh, Catal. Commun. 12 (2011) 1104–1108.
[10] H. Yamamoto, H. Yano, H. Kouchi, Y. Obora, R. Arakawa, H. Kawasaki, Nanoscale 4 (2012) 4148–4154.
[11] Z.Y. Ji, X.P. Shen, G.X. Zhu, H. Zhou, A.H. Yuan, J. Mater. Chem. 22 (2012) 3471–3477.
[12] A.A. Balandin, S. Ghosh, W.Z. Bao, I. Calizo, D. Teweldebrhan, F. Miao, C.N. Lau, Nano Lett. 8 (2008) 902–907.
[13] A.K. Geim, Science 324 (2009) 1530–1534.
[14] A.K. Geim, K.S. Novoselov, Nat. Mater. 6 (2007) 183–191.
[15] K.S. Kim, Y. Zhao, H. Jang, S.Y. Lee, J.M. Kim, K.S. Kim, J.H. Ahn, P. Kim, J.Y. Choi, B.H. Hong, Nature 457 (2009) 706–710.
[16] S. Stankovich, D.A. Dikin, G.H.B. Dommett, K.M. Kohlhaas, E.J. Zimney, E.A. Stach, R.D. Piner, S.T. Nguyen, R.S. Ruoff, Nature 442 (2006) 282–286.
[17] D.R. Dreyer, S. Park, C.W. Bielawski, R.S. Ruoff, Chem. Soc. Rev. 39 (2010) 228–240.
[18] G. Eda, G. Fanchini, M. Chhowalla, Nat. Nanotechnol. 3 (2008) 270–274.
[19] A. Buchsteiner, A. Lerf, J. Pieper, J. Phys. Chem. B 110 (2006) 22328–22338.
[20] K. Jasuja, V. Berry, ACS Nano 3 (2009) 2358–2366.
[21] X.Z. Zhou, X. Huang, X.Y. Qi, S.X. Wu, C. Xue, F.Y.C. Boey, Q.Y. Yan, P. Chen, H. Zhang, J. Phys. Chem. C 113 (2009) 10842–10846.
[22] W. Wang, J. Yu, Q. Xiang, B. Cheng, Appl. Catal. B 119–120 (2012) 109–116.
[23] E. Antolini, Appl. Catal. B 123–124 (2012) 52–68.
[24] P. Shi, R. Su, F. Wan, M. Zhu, D. Li, S. Xu, Appl. Catal. B 123–124 (2012) 265–272.
[25] C.J. Chen, D.H. Chen, Chem. Eng. J. 180 (2012) 337–342.
[26] B.H. Lai, D.H. Chen, Acta Biomater. 9 (2013) 7556–7563.
[27] B.H. Lai, D.H. Chen, Acta Biomater. 9 (2013) 7573–7579.
[28] B.H. Lai, Y.R. Lin, D.H. Chen, Chem. Eng. J. 223 (2013) 418–424.
[29] J.R. Robinson, S.M. Tabakman, Y. Liang, H. Wang, H.S. Casalongue, D. Vinh, H. Dai, J. Am. Chem. Soc. 133 (2011) 6825–6831.
[30] Z.M. Markovic, L.M. Harhaji-Trajkovic, B.M. Todorovic-Markovic, D.P. Kepic, K.M. Arsikin, S.P. Jovanovic, A.C. Pantovic, M.D. Dramicanin, V.S. Trajkovic, Biomaterials 32 (2011) 1121–1129.
[31] W. Zhang, Z. Guo, D. Huang, Z. Liu, X. Guo, H. Zhong, Biomaterials 32 (2011) 8555–8561.
[32] G. Liu, Y. Wang, F. Qiu, L. Li, L. Jiao, H. Yuan, J. Mater. Chem. 22 (2012) 22542–22549.
[33] B. Li, H. Cao, J. Yin, Y.A. Wu, J.H. Warner, J. Mater. Chem. 22 (2012) 1876–1883.
[34] L.R. Zhang, J. Zhao, M. Li, H.T. Ni, J.L. Zhang, X.M. Feng, Y.W. Ma, Q.L. Fan, X.Z. Wang, Z. Hu, W. Huang, New J. Chem. 36 (2012) 1108–1113.
[35] Ö. Metin, S.F. Ho, C. Alp, H. Can, M.N. Mankin, M.S. Gültekin, M. Chi, S. Sun, Nano Res. 6 (2013) 10–18.
[36] Z. Wang, Y. Du, F. Zhang, Z. Zheng, Y. Zhang, C. Wang, J. Solid State Electrochem. 17 (2013) 9–107.
[37] W.S. Hummers Jr., R.E. Offeman, J. Am. Chem. Soc. 80 (1958) 1339.
[38] S.H. Wu, D.H. Chen, J. Colloid Inter. Sci. 259 (2003) 282–286.
[39] B.D. Cullity, S.R. Stock, Elements of X-Ray Diffraction, third ed., Prentice-Hall Inc., 2001, pp. 167–171.
[40] A.C. Ferrari, J.C. Meyer, V. Scardaci, C. Casiraghi, M. Lazzeri, F. Mauri, S. Piscanec, D. Jiang, K.S. Novoselov, S. Roth, A.K. Geim, Phys. Rev. Lett. 97 (2006) 187401.
[41] C. Stampfer, F. Molitor, D. Graf, K. Ensslin, A. Jungen, C. Hierold, L. Wirtz, Appl. Phys. Lett. 91 (2007) 241907.
[42] F. Tuinstra, J.L. Koenig, Raman spectrum of graphite, J. Chem. Phys. 53 (1970) 1126–1130.
[43] S. Stankovich, D.A. Dikin, R.D. Piner, K.A. Kohlhaas, A. Kleinhammes, Y. Jia, Y. Wu, S.T. Nguyen, R.S. Ruoff, Carbon 45 (2007) 1558–1565.
[44] C. Xu, X. Wang, J.W. Zhu, J. Phys. Chem. C 112 (2008) 19841–19845.
[45] Y.W. Zhang, S. Liu, W.B. Lu, L. Wang, J.Q. Tian, X.P. Sun, Catal. Sci. Technol. 1 (2011) 1142–1144.
[46] R. Leary, A. Westwood, Carbon 49 (2011) 741–772.
[47] J. Li, C.Y. Liu, Y. Liu, J. Mater. Chem. 22 (2012) 8426–8430.
[48] X.J. Wu, X.C. Zeng, Nano Lett. 9 (2009) 250–256.
[49] B.G. Baker, B.B. Johnson, G.L.C. Maire, Surf. Sci. 24 (1971) 572–586.